Optics and Lasers in Engineering 159 (2022) 107204

Contents lists available at ScienceDirect

Optics and Lasers in Engineering

journal homepage: www.elsevier.com/locate/optlaseng

Ferroelectric liquid-crystal modulator with large switching rotation angle for polarization-independent binary phase modulation

Esther Nabadda[a], Noureddine Bennis[b], Michał Czerwinski[b], Aleksandra Walewska[b], Leszek R. Jaroszewicz[b], María del Mar Sánchez-López[a,c,*], Ignacio Moreno[a,d]

[a] Instituto de Bioingeniería. Universidad Miguel Hernández de Elche, Elche E-03202, Spain
[b] Faculty of New Technologies and Chemistry. Military University of Technology, Warsaw 00-908, Poland
[c] Departamento de Física Aplicada. Universidad Miguel Hernández de Elche, Elche E-03202, Spain
[d] Departamento de Ciencia de Materiales, Óptica y Tecnología Electrónica, Universidad Miguel Hernández de Elche, Elche E-03202, Spain

ARTICLE INFO

Keywords:
Ferroelectric liquid-crystal
Polarization
Phase modulation

ABSTRACT

In this work a ferroelectric liquid crystal (FLC) modulator with a non-standard large switching rotation angle, close to 90°, is fabricated and characterized. The modulator acts as a switchable wave-plate with an in-plane rotation of the principal axis under the action of a bipolar voltage. In the ideal situation of half-wave retardance, the device is shown to behave as a binary π phase modulator independently of the input state of polarization. We provide physico-chemical properties of the liquid crystalline mixture used to fabricate the FLC modulator with such large switching angle. The characterization method of the device optical properties is presented, which allows the localization of the two LC stable states, the unambiguous determination of the rotation angle, and the evaluation of the spectral retardance function. We demonstrate the polarization-independent π phase shift using an adapted Young's type interferometer for real-time measurements, where we further analyze the operational frequency limits of the device. This FLC operational mode can be exploited to produce binary-phase polarization-independent diffractive optical elements.

1. Introduction

Ferroelectric liquid crystals (FLC), also known as chiral smectic or smectic *C phase (Sm*C), have a long history and they have been used to fabricate many different types of optical modulators [1]. In comparison with the more common nematic LC modulators, they present bistable faster response and low consumption. In their typical configuration as surface stabilized ferroelectric liquid-crystals (SSFLC) they operate as a switchable linear retarder (waveplate) with two stable in-plane orientations of the LC director. These properties make them very interesting elements for fast optical switches [2–4]. They have been employed as achromatic phase shifters [5], optical depolarizers [6] and for designing polarimetric instruments [7,8]. Recent advances include using them to fabricate fast refocusing lenses [9] or LiDAR systems [10]. A recent review of the state of the art of FLC modulators can be found in [11].

A major application of FLCs is on the production of liquid-crystal displays (LCD), where their fast response is especially useful to reduce motion blur and to achieve field sequential color (FSC) displays. Ferroelectric LCDs (FLCDs) are typically designed with a retardance of $\phi = 180^{\circ}$, i.e., as a half-wave plate (HWP), and with in-plane switching rotation angle of $\theta = 45^{\circ}$. In this situation, if the FLC modulator is illuminated with linearly polarized light, it provides output light with two orthogonal linear states of polarization (SOP). These can be converted into a maximum contrast binary light intensity modulation by setting an analyser at the output, crossed to one of the two emerging states [12,13].

In this work, instead of regarding the display application, we are more interested in FLCDs as phase-only spatial light modulators (SLM) for diffractive and/or adaptive optics. FLC-SLMs have been used for a long time to display binary phase diffraction gratings [14] and binary-phase computer generated holograms [15]. Although not as popular as nematic LC-SLMs, FLC SLMs are also commercially available [16] and they have been applied in systems where a fast modulation response is required, as for instance laser speckle reduction [17], microscopy with structured illumination [18,19] or optogenetic stimulation [20]. These FLC-SLM commercial devices, though, are fabricated with $\theta \approx 45^{\circ}$ (or less) switching rotation angle of the FLC director. Although a binary π phase modulation operational scheme can be obtained with these modulators by properly orienting an output analyzer to filter the modulated beam [21], this is at the expense of losing light efficiency.

Here we analyze the properties of a FLC modulator with $\theta \approx 90^{\circ}$ switching angle. We illustrate how this device provides, when the LC layer is a half-wave retarder, a binary π phase modulation for any input

* Corresponding author at: Instituto de Bioingeniería, Universidad Miguel Hernández de Elche, Elche E-03202, Spain.
E-mail address: mar.sanchez@umh.es (M.d.M. Sánchez-López).

https://doi.org/10.1016/j.optlaseng.2022.107204
Received 20 March 2022; Received in revised form 24 June 2022; Accepted 26 July 2022
Available online 4 August 2022

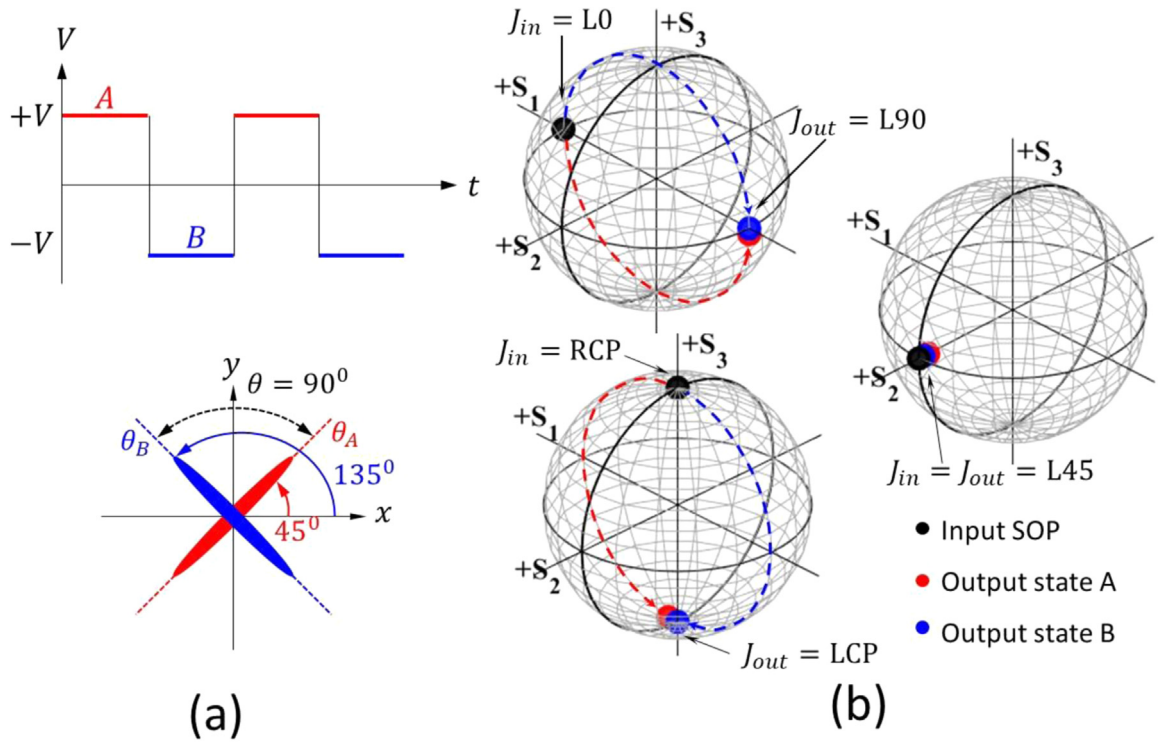

Fig. 1. Ideal FLC modulator for binary π phase modulation with maximum efficiency: (a) Switching of the FLC director between stable states A and B. (b) Evolution on the PS showing the output polarization for various input SOP.

SOP and with maximum light conversion efficiency. Since the binary π phase modulation regime occurs for any SOP, it could be operated even with unpolarized light. Consequently, light efficiency can be further improved since there is no need to use polarizers. Although this configuration was proposed many years ago [22–25], and LC materials with high tilt angle (like the CS2005 or the CDRR8 mixture) were investigated [26], the SLM industry has not considered it. With this work we would like to stimulate the recovery of this old idea. In addition, the in-plane rotation of the FLC modulators can be regarded to imprint a geometric phase to the input beam, also known as the Pancharatnam-Berry phase, thus being useful to design a new generation of geometric-phase-based diffractive optical elements [27]. Therefore, FLC modulators can be viewed as binary geometric phase elements as well.

After this introduction, the paper is organized as follows: in the next section we present the theory of the ideal FLC device and provide the physical insight of the SOP transformations described within the Poincaré sphere formalism. In Section 3, the physico-chemical properties of the LC mixture used to fabricate the FLC cell modulator are described. In Section 4 we provide a procedure for the complete optical characterization of the device light modulation properties. The time response is presented in Section 5. Section 6 further illustrates the binary π phase modulation for any input SOP by means of an adapted experimental Young's type interferometer arrangement [28]. Finally, the conclusions of the work are given in the last section.

2. Operation of a FLC modulator with 90° rotation and 180° retardance

In this section we analyze the operation of the FLC modulator considering the ideal situation where the retardance is $\phi = 180^\circ$ i.e., it is a half wave plate (HWP), with the LC director switching between two stable positions A and B (θ_A and θ_B), where the switching rotation angle is $\theta = \theta_B - \theta_A = 90^\circ$. Note that the rotation angle is $\theta = 2\vartheta_T$, twice the so-called tilt angle ϑ_T.

Considering the Jones matrix formalism for polarized light, and assuming that the FLC layer acts as a HWP, the FLC modulator at position A is described by

$$\mathbf{M}_A = \begin{bmatrix} \cos 2\theta_A & \sin 2\theta_A \\ \sin 2\theta_A & -\cos 2\theta_A \end{bmatrix}, \tag{1}$$

while for FLC position B the Jones matrix is

$$\mathbf{M}_B = \begin{bmatrix} \cos 2\theta_B & \sin 2\theta_B \\ \sin 2\theta_B & -\cos 2\theta_B \end{bmatrix} = -\begin{bmatrix} \cos 2\theta_A & \sin 2\theta_A \\ \sin 2\theta_A & -\cos 2\theta_A \end{bmatrix} = -\mathbf{M}_A, \tag{2}$$

where the relation $\theta_B = \theta_A + 90^\circ$ was used. Therefore, since $\mathbf{M}_B = -\mathbf{M}_A$, for any input polarization, the two output SOPs are identical except for a minus sign which implies a π phase shift between them.

Fig. 1 illustrates this situation. In Fig. 1(a) two FLC director orientations $\theta_A = 45^\circ$ and $\theta_B = 135^\circ$ are drawn, thus leading to $\theta = 90^\circ$, corresponding to the two values of a bipolar addressed electrical signal. The two output SOPs suffer a transformation with respect to the input SOP (except for the eigenstates, i.e., the linear polarised states parallel or crossed to the FLC director). However, since the FLC modulator is a HWP, the two emerging SOPs are the same for the two positions A and B. These transformations can be visualized on the Poincaré sphere (PS) [29]. The PS is a geometrical representation of all SOPs, where the latitude coordinate is directly related to the light ellipticity and the longitude coordinate is directly related to the polarization azimuth. The two circularly SOPs are the poles of the PS, while the linear SOPs lie in the equator. The interest of the PS in describing retarder elements (as the FLC modulator) is that the action of the device on any input SOP is a rotation of the PS around the axis defined by the two eigenstates, with an angle equal to the retardance. In this case of a HWP FLC modulator, the PS rotates an angle equal to $\phi = 180^\circ$. Fig. 1(b) illustrates these transformations. Given the orientations of the FLC director in Fig. 1(a), both A and B positions share the same eigenstates; namely, the linear states oriented at 45° and 135°. Therefore, the PS rotation is in both cases around the S_2 axis. However, the rotation of the FLC director interchanges the fast and slow axes of the retarder and, consequently, the PS rotates in

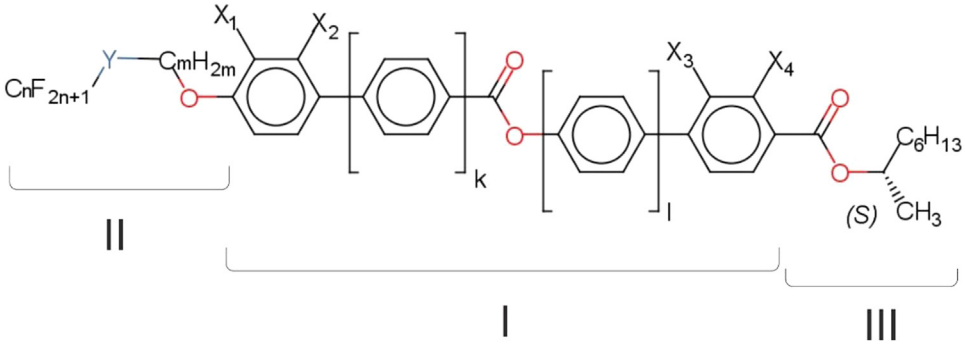

Fig. 2. Chemical structure of the components of the W-212 mixture used in this work.

the opposite direction. This is shown in Fig. 1(b) for various input SOPs (black dots): a linear horizontal SOP (located on the $+S_1$ axis), a linear SOP oriented at 45° (located on the $+S_2$ axis) and a right circular SOP (RCP) (located on the $+S_3$ axis, at the north pole). Although the final SOP is the same for both A and B positions, the trajectory on the PS has opposite direction, which provides an opposite geometric phase between the two emerging SOPs. Even in the case of an input linear SOP oriented at 45°, which does not suffer any polarization transformation, there is a π phase difference originated from the switch between the fast and slow axes of the FLC retarder.

3. Structure and properties of the FLC mixture and fabrication of the cell

The FLC cell was produced at the Military University of Technology (Warsaw). Here the details on the preparation of the LC mixture and on the device fabrication are provided.

3.1. Preparation of a multicomponent FLC mixture

The LC mixture used in this work was proposed and developed at the Institute of Chemistry (Military University of Technology). This mixture is intended to achieve all the properties required in FLC applications, such as broad temperature range of the ferroelectric phase, relatively low melting point and optimized ferroelectric electro-optical response. The mixture was prepared according to a procedure based on mixing selected chiral compounds with ferroelectric and antiferroelectric properties, with the scope of finding a composition which presents a frustrated ferroelectric phase as in [30]. The components of the obtained W-212 mixture are made up of a rigid ring structure formed by biphenyl benzoate or phenyl biphenylate structure (I), nonchiral partially fluorinated alkoxy terminal chain in one side of molecules (II) and chiral 1-methylheptyloxy chain (III), which is connected to the rigid core using carboxylate bridge in the other side (Fig. 2). This structure is like those shown in [31], where homologue mixtures to W-212 with very short helical pitch were reported. To ensure uniform alignment in the electro-optical cell with thickness higher than 2mm, a small amount of racemic chiral dopant was added to increase the helical pitch in the final W-212 mixture. This mixture has been synthesized according to the procedure found in the original publication [32].

3.2. Physico-chemical properties of the W-212 mixture

We show next results of the phase transition temperatures, the director tilt angle and spontaneous polarization measurements for the W-212 mixture. Increasing the temperature, a variety of thermodynamically stable intermediary states between crystal (Cr) and isotropic (Iso) state are observed. These intermediate mesophases are stable thermotropic liquid crystalline states termed enantiotropic [33]. Using differential scanning calorimetry (DSC) and polarizing microscopy techniques, the following phase transitions were observed upon heating at 2 °C/min:

$$\mathrm{Cr} \underset{10°\mathrm{C}}{\rightarrow} \mathrm{SmC}^* \underset{99.8-101.5°\mathrm{C}}{\rightarrow} \mathrm{SmA}^* \underset{117.5-126.0°\mathrm{C}}{\rightarrow} \mathrm{ISO}$$

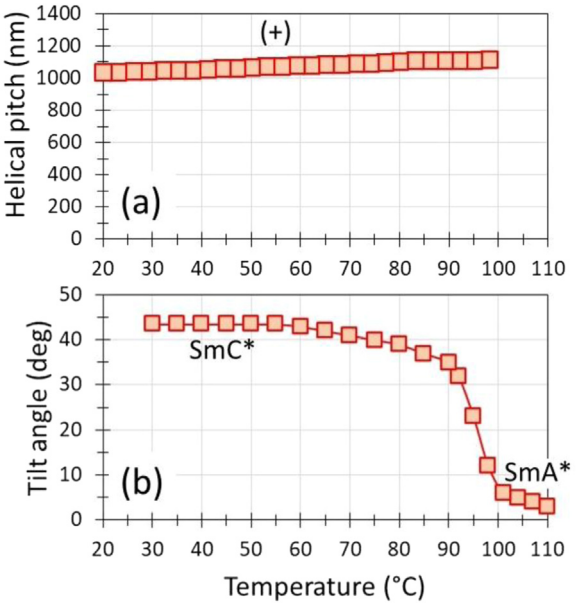

Fig. 3. (a) Temperature dependence of the helical pitch for the W-212 mixture. The sense of the helical twist is indicated by "+" for the right-handed helix. (b) Tilt angle as a function of temperature.

Bulk states in W-212 exhibit helical structures induced by the twisting power due to chirality. The helical pitch P was determined in the temperature range that covers the tilted chiral smectic phase SmC* by measuring the transmittance spectra with a spectrophotometer of 360–3000 nm spectral range. P is calculated with the relation $P = \lambda_C/n$, where λ_C is the central wavelength of the reflection band and n is the average refractive index. The W-212 mixture was placed on a glass plate coated with a surfactant, thus promoting the homeotropic orientation of the molecular director while the other surface of the specimen was left free. More experimental details of the helical pitch and helical twist sense measurements were reported in previous works [34–36]. Here we present the temperature dependence of the pitch for the W-212 mixture, which slowly increases with temperature in the SmC* phase, reaching a maximum value about 1150 nm at 100 °C (Fig. 3(a)), just below the transition temperature from SmC* to SmA*.

To measure the tilt angle ϑ_T (half the switching rotation angle of the LC director), the LC was introduced in cells aligning the molecular director parallel to the substrate surface. In this case, the cell consists of two ITO-coated glass that are patterned to give a 7×7 mm^2 electrode area. The glass surface was processed with a Nylon 6 as aligning material and unidirectionally rubbed prior to cell assembly, in order to produce

a homogenous alignment. Then, the two-substrate glasses were joined together with an epoxy glue containing 2.5 mm spacers. The FLC material was placed at one of the cell's edges. The cell was then heated until the material was in the isotropic phase, to allow the material flow inside the cell by capillary forces. Furthermore, the cell was cooled down at controlled rate (0.1 ˚C/min) while applying an AC electric field to form the aligned ferroelectric liquid crystal at room temperature.

The helical structure is suppressed by the surface effect resulting in a molecular tilting plane parallel to the surface, thus obtaining the surface-stabilized ferroelectric liquid crystal (SSFLC) configuration. The cell was placed in a temperature and environmental control stage (Linkam THMS 600) compatible with a polarization optical microscope (Biolar PI-PZO). When the cell is under DC electric field the material aligns in a single direction. The tilt angle $\vartheta_T = \theta/2$ is typically measured by placing the FLC cell between the crossed polarizers of the microscope and orienting it such that extinction is obtained. In this orientation the optical axis of the material is parallel to one of the polarizers. By reversing the polarity of the applied DC field, the FLC molecules reorient, and the cell appears brighter. The FLC cell is rotated on the microscope stage to bring the dark state of the cell back again. This rotation is thus the switching angle θ and $\vartheta_T = \theta/2$ is the tilt angle. However, in the case of a perfect value $\theta = 90^{\circ}$ the dark state would remain after reversing the field. Nevertheless, we could apply the procedure following the temperature variations and Fig. 3(b) shows the results for the measured tilt angle. They show that the tilt angle rises rapidly into the SmC* phase on cooling from the SmA* phase before saturating at 43˚ in the broad temperature range (below 55 ˚C) of the ferroelectric phase. Following a similar procedure, the retardance was measured, and the birefringence of the material could be estimated to be $\Delta n = 0.11 \pm 0.01$, with no significant variation in the SmC* phase temperature range between 30 ˚C and 80 ˚C.

The magnitude of the tilt angle of the LC molecules in the ferroelectric phase has an influence on the value of the spontaneous polarization. Usually, the higher the tilt angle the higher the spontaneous polarization and the material could reorient faster in an optical modulator. Accordingly, it is important to determine the magnitude de the spontaneous polarization. This can be measured using a triangular waveform voltage, in this case with a frequency of 50 Hz. The current through the circuit was monitored and the polarization was determined by measuring the charge produced upon polarization reversal (Fig. 4(a)). This was measured for different temperatures and the dependence shown in Fig. 4(b) exhibits a behavior similar to the tilt angle, increasing its value as the temperature is reduced, reaching about 115nC/cm^2 at 25 ˚C.

Finally, the bistable nature of the FLC cell is analyzed. The cell is now addressed with a low frequency triangular voltage signal of 20 Vpp and 0.1 Hz. Fig. 4(c) shows the optical transmittance between crossed polarizers as a function of the applied voltage, both for the rise (black curve) and for the fall (brown curve) of the applied signal. As described previously, the material employed in this work is a frustrated ferroelectric phase [31] and the transmittance exhibits a ferroelectric loop with anomalous hysteresis showing a W-shape, as demonstrated in Fig. 4(c).

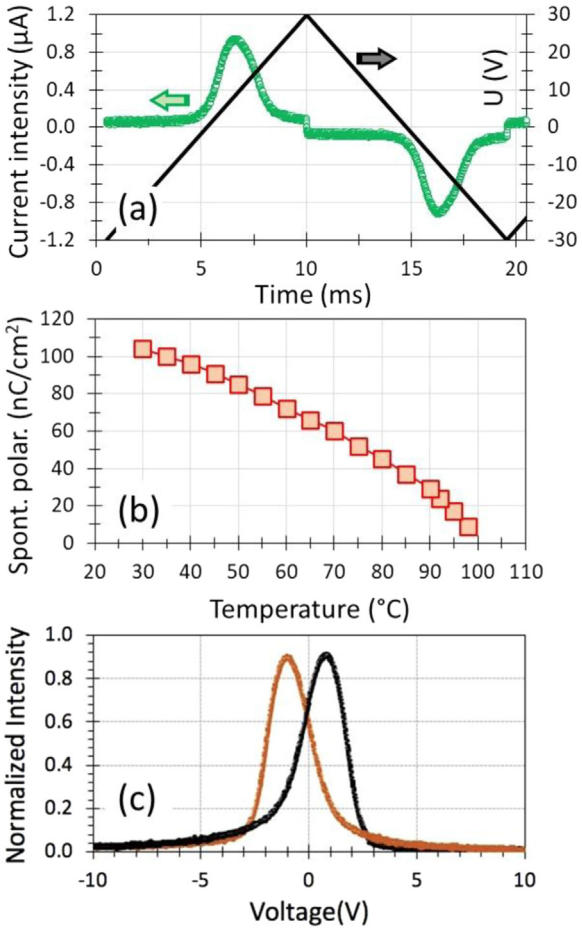

Fig. 4. (a) Polarization switching current response for the W-212 mixture by applying a triangular waveform voltage of 50 Hz. (b) Temperature dependence of the spontaneous polarization for the W-212 mixture. (c) Measured hysteresis loop (black and brown curves correspond respectively to the rise and fall of the low frequency triangular voltage signal).

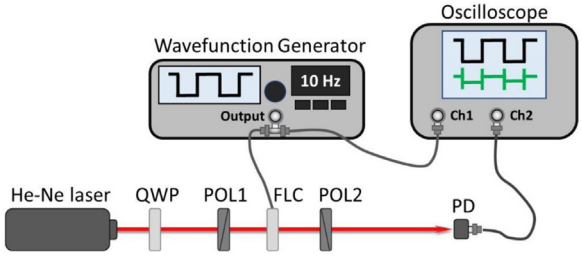

Fig. 5. Scheme of the optical setup. QWP: quarter-wave plate; POL: linear polarizer; PD: photodetector.

4. Characterizing the optical parameters of the FLC modulator

These previous experiments require the use of equipment specially designed for the characterization of LC materials. However, it is a quite common situation, especially when employing LC commercial devices, that the user does not have access to the fabrication details. In these situations, it is necessary to develop reverse engineering techniques aiming at determining the physical parameters that influence the optical modulation properties. In this section we present the set of reverse engineering procedures that we have performed to experimentally verify the physical parameters of the FLC modulator described in the last section. Namely, the orientation of the LC director, the LC layer retardance (ϕ) and the switching angle (θ). These experiments require relatively simple equipment and can be done even without knowledge whatsoever of the fabrication parameters.

4.1. Locating the FLC director and the switching angle

We first searched for the orientation of the FLC director following a similar procedure as in [13,21]. Fig. 5 shows a scheme of the optical setup. The system is illuminated with a He-Ne laser beam of wavelength 632.8 nm. Since the laser is linearly polarized, a quarter-wave plate (QWP) was added to produce circularly polarized light. Then, the polarizer – FLC modulator – analyser system was placed behind. Both polarizers were mounted on rotating mounts. Having generated circularly polarized light ensures that the input polarizer can be rotated to

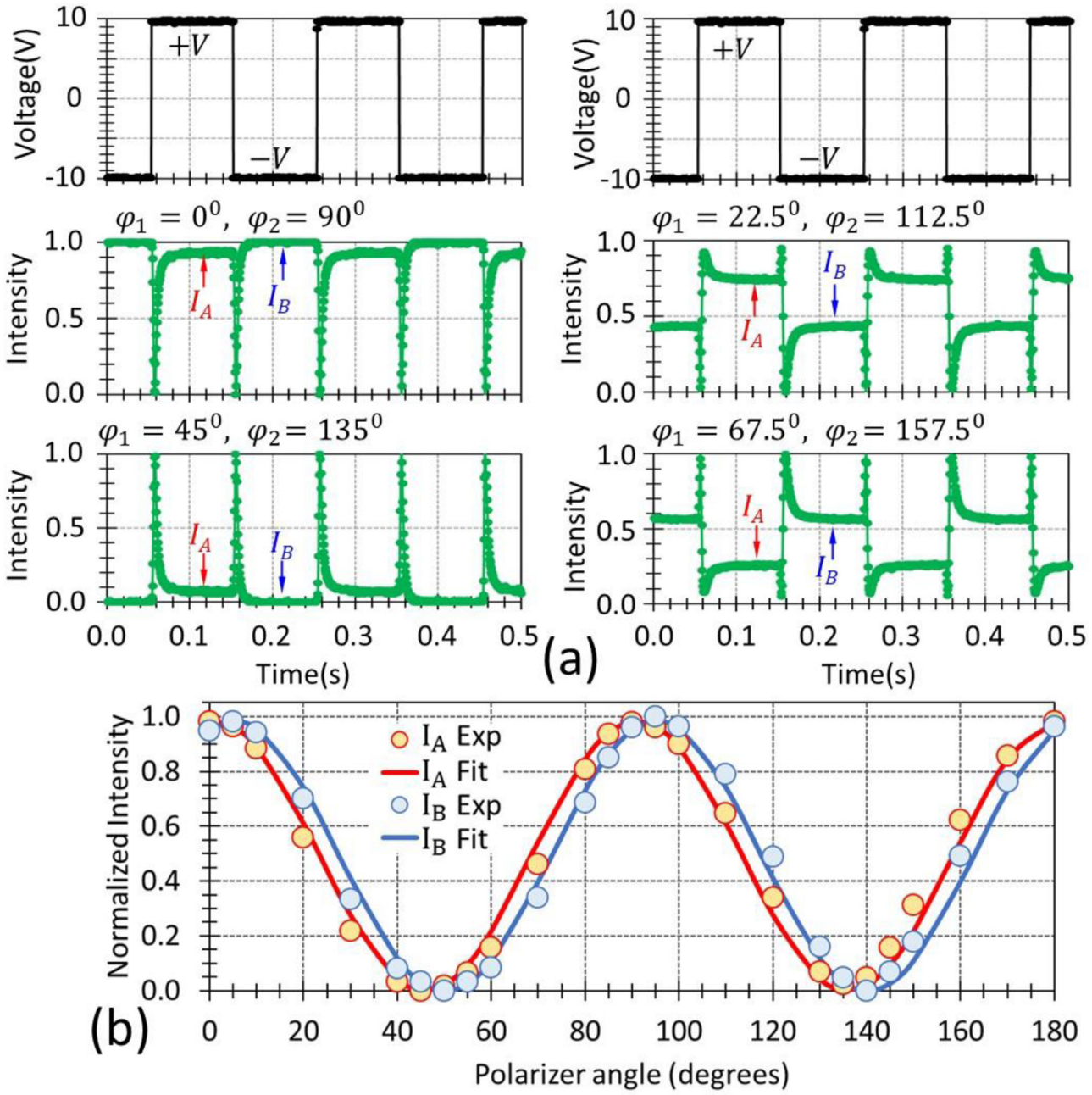

Fig. 6. FLC modulator between crossed polarizers (a) Captured normalized intensity signal for input polarizer angle at $\varphi_1 = 0$, 22.5°, 45° and 67.5°. (b) Normalized intensity transmission for the two FLC stable states (A and B) as a function of the input polarizer angle.

arbitrary angles, while maintaining the input intensity on the FLC modulator. A photodetector (Newport 818-SL) captures the transmitted intensity and displays it on an oscilloscope with temporal resolution. The FLC modulator was addressed with a bipolar voltage of 10 Hz, 20Vpp and null DC value from a wavefunction generator. The oscilloscope displays simultaneously the addressed signal and the signal detected on the photodetector (PD).

For crossed polarizers the normalized transmitted signal (i.e., the ratio between the intensity after POL2 and the intensity incident on the FLC modulator) takes the form [21]:

$$T_{cross} = \sin^2(2\alpha)\sin^2\left(\frac{\phi}{2}\right), \tag{3a}$$

where $\alpha = \varphi_1 - \theta_{A/B}$ denotes the difference between the input polarizer angle (φ_1) and the FLC principal axis, which takes the angles $\theta_{A/B}$ for the two stable positions of the FLC director. For normalization purposes, the same experiment was performed with parallel polarizers, where the normalized transmission is given by

$$T_{par} = 1 - \sin^2(2\alpha)\sin^2\left(\frac{\phi}{2}\right). \tag{3b}$$

According to Eqs. 3(a), when the input polarizer is either parallel ($\alpha = 0°$) or perpendicular ($\alpha = 90°$) to the LC director, the transmission is null for crossed polarizers. Maximum transmittance for crossed polarizers occurs when the relative orientation between the input polarizer and the LC director is set at $\alpha = 45°$. In this latter situation, the transmittance for crossed polarizers is equal to $\sin^2(\phi/2)$ and reaches 100% transmission when the retardance is $\phi = 180°$. Therefore, by fitting the experimental transmittance for crossed polarizers we will retrieve the retardance of the FLC cell.

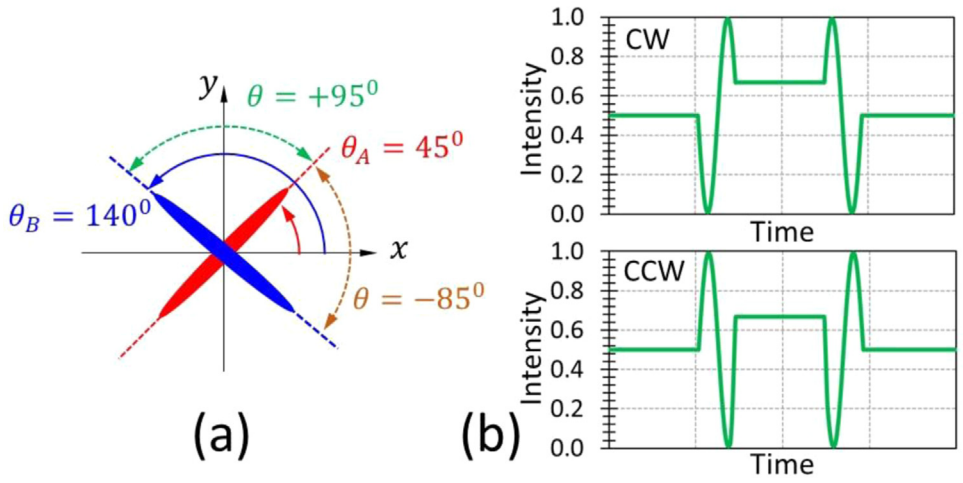

Fig. 7. (a) Rotation of the FLC director in the real situation. (b) Numerical simulation of the normalized transmission for clockwise and counter-clockwise (CCW) rotation of the FLC director with the cell placed between two crossed linear polarizers and input polarizer at 22.5°.

Fig. 6(a) presents the experimental normalized transmitted signal of the FLC cell placed between crossed polarizers, as a function of time. The black curves indicate the bipolar voltage signal addressed to the cell while the green dots refer to the signal measured by the photodetector and captured in the oscilloscope. This signal shows two stable intensity values (I_A and I_B) that correspond to the two applied voltage levels, with short transition peaks in between. These peaks correspond to the transient response where the LC director reorients, and they were studied in detail in the past [37,38] where they were shown to be related to soliton type switching which occurs under fixed boundary conditions. These transient states can be used to provide continuous amplitude or phase modulation with FLC modulators [39]. Here, however, we concentrate on the standard operation as binary modulators.

In the ideal situation described in Section 2 (90° switching angle and 180° retardance), the two stable intensity values should be identical. However, their slight difference indicates that the modulator parameters are close to the ideal conditions, although they are not perfect. Fig. 6(a) shows four captures where the input polarizer was oriented in the laboratory framework at angles $\varphi_1 = 0°$, 22.5°, 45° and 67.5° while the analyzer was kept crossed at angles $\varphi_2 = 90°$, 112.5°, 135° and 157.5° respectively.

Similar measurements were taken for different orientations of the input polarizer (φ_1), while rotating the analyzer to always keep them crossed. At each angle φ_1, we recorded the two stable intensity values (I_A and I_B) occurring for the positive and negative level of the applied voltage. For normalization purposes, the equivalent procedure was taken setting the FLC between parallel polarizers. Fig. 6(b) represents the normalized transmission (in the crossed configuration) as a function of the input polarizer angle, for the two stable FLC positions A and B. The dots represent the experimental data while the continuous curves were obtained from fitting these data to Eq. 3(a). The two curves display the expected oscillating behavior, with maximum transmission close to 100%, thus verifying that the retardance is very close to the ideal value of $\phi = 180°$. Two possible retardance values were obtained from the best fit curves: $\phi = 164°$ or $\phi = 196°$. This ambiguity stems from the $\sin^2(\phi/2)$ term in Eq. (3), but it can be resolved with a spectral technique [40], as will be shown next.

Note that the two curves in Fig. 6(b) are slightly shifted laterally: while the red curve (A) minima lie at $\varphi_{1A} = 45°$ and $\varphi_{1A} = 135°$, the blue curve (B) minima are located at $\varphi_{1B} = 50°$ and $\varphi_{1B} = 140°$. These minima were determined from the best fit curves, with an estimated uncertainty of one degree. As discussed earlier, the transmission is null when the input polarizer is aligned parallel or perpendicular to the FLC director. Therefore, the angles of null transmission gives us the orientations of the neutral axes of the FLC cell in the two stable positions. These stable positions of the fabricated FLC modulator are drawn in Fig. 7(a). In the ideal situation of $\theta = 90°$ rotation angle, the two curves in Fig. 6(b) should overlap. The slight shift is an indication that the ideal value was not achieved in fabrication. From the location of the minima we obtain a rotation angle of either $\theta = 85°$ or $\theta = 95°$, depending on the sense of rotation. Although the previous analysis shown in Fig. 3(b) indicates that the correct value is $\theta = 85°$, next we describe an additional experiment to confirm this hypothesis and determine the sense of rotation of the FLC director.

4.2. Determining the sense of rotation

Considering the positive voltage of the input square signal and the negative voltage as yielding the stable states A and B respectively, the FLC director can rotate either clockwise (CW) or counterclockwise (CCW). The sense of rotation of the FLC director can be derived from the transitions observed in the oscillograms in Fig. 6(a). Fig. 7(b) shows two numerical simulations for the two possible rotation directions, where the input polarizer is set at an angle $\varphi_1 = 22.5°$. We select this configuration since it corresponds to one of the experimental captures in Fig. 6(a) which shows intensity transmission values around $T = 0.5$ for both FLC stable states with transitions in the form of narrow peaks that transit between zero and 100%. Simulations were run considering $\phi = 164°$ retardance and the two possible values of θ with both sense of rotation. In the transitions, the peak goes first to zero and then to 100% transmission, or the opposite, depending on the sense of rotation of the FLC director. Comparing the direction of these transition peaks in the experiments in Fig. 6(a), we conclude that the FLC director rotates clockwise through an angle of $\theta = +85°$.

4.3. Characterization of the spectral retardance

As mentioned in Section 4.1, an ambiguity remains in the retardance, which can take values $\phi = 164°$ or $\phi = 196°$ that equally fit the experimental data. Spectral measurements can be performed to easily resolve this ambiguity [40]. For that purpose, the He-Ne laser in the optical setup of Fig. 5 is replaced by a broadband light source (a quartz tungsten halogen lamp from Oriel, model 66,882). The FLC cell is placed between crossed and parallel linear polarizers, oriented at an angle $\alpha = 45°$ relative to the principal axis of the retarder. The transmitted light is captured by a Stellar-Net spectrometer (STN-BLK-C-SR). Again, a bipolar signal of 20 Vpp is applied to the modulator, now with a very low frequency of only 1 Hz to make possible the capture of the output signal on the spectrometer.

Fig. 9(a) shows the normalized transmission curves in the range from 500 to 800 nm for stable position A (equivalent curves were obtained for position B). These curves show the typical transmission of a zero-order

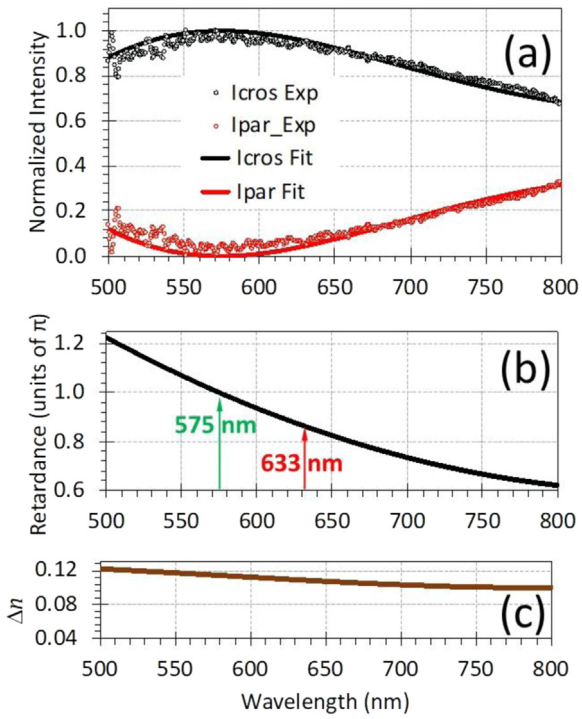

Fig. 8. (a) Normalized spectral intensity transmission of the FLC modulator between crossed and parallel polarizers oriented at 45° with respect to the LC director. (b) Spectral retardance function that best fits the experimental data. (c) Spectral birefringence $\Delta n(\lambda)$.

half-wave plate [40] with a very low transmission for crossed polarizers, below 0.1, in a wide spectral range between 530 nm and 650 nm. From Eqs. 3(a)–3(b), the spectral retardance function can be derived from the transmission data as

$$\phi(\lambda) = 2\arctan\left[\sqrt{\left(\frac{T_{cross}(\lambda)}{T_{par}(\lambda)}\right)}\right]. \tag{4}$$

Since the FLC modulator is composed of a single LC layer, the retardance must follow a relation $\phi(\lambda) = \frac{2\pi}{\lambda}\Delta n \cdot t$, where Δn is the LC birefringence and t is the LC layer thickness. Therefore, $\phi(\lambda)$ typically follows a monotonically decreasing function with the λ. As it was done in [40], we employ a Cauchy equation for the spectral retardance and use it to fit these experimental intensity curves. Fig. 8(a) shows also the best fit obtained for the normalized intensity in crossed and parallel configurations, while the function $\phi(\lambda)$ that best fits the experimental data is plotted in Fig. 8(b). According to this result the retardance obtained for the $\lambda = 633$ nm wavelength is below π, thus verifying the previously obtained value $\phi = 164°$. The ideal HWP retardance would be obtained at 575 nm. Nevertheless, we keep considering operation at 633 nm since it corresponds to the common wavelength of a standard He-Ne laser and the 164° retardance is close enough to the ideal value. Finally, Fig. 8(c) shows the wavelength variation of the birefringence Δn, which is calculated from the previous result as $\Delta n = \lambda\phi(\lambda)/2\pi t$, assuming the LC thickness value of $t = 2.5$ microns. The value $\Delta n = 0.109$ is obtained for $\lambda = 633$ nm, thus confirming previous results.

5. Characterization of the time response

For purposes of its effective performance, it is important to calibrate the frequency limit of the FLC modulator. We then apply a square signal of 20Vpp and increasing frequency up to 200 Hz. Fig. 9 shows the effect

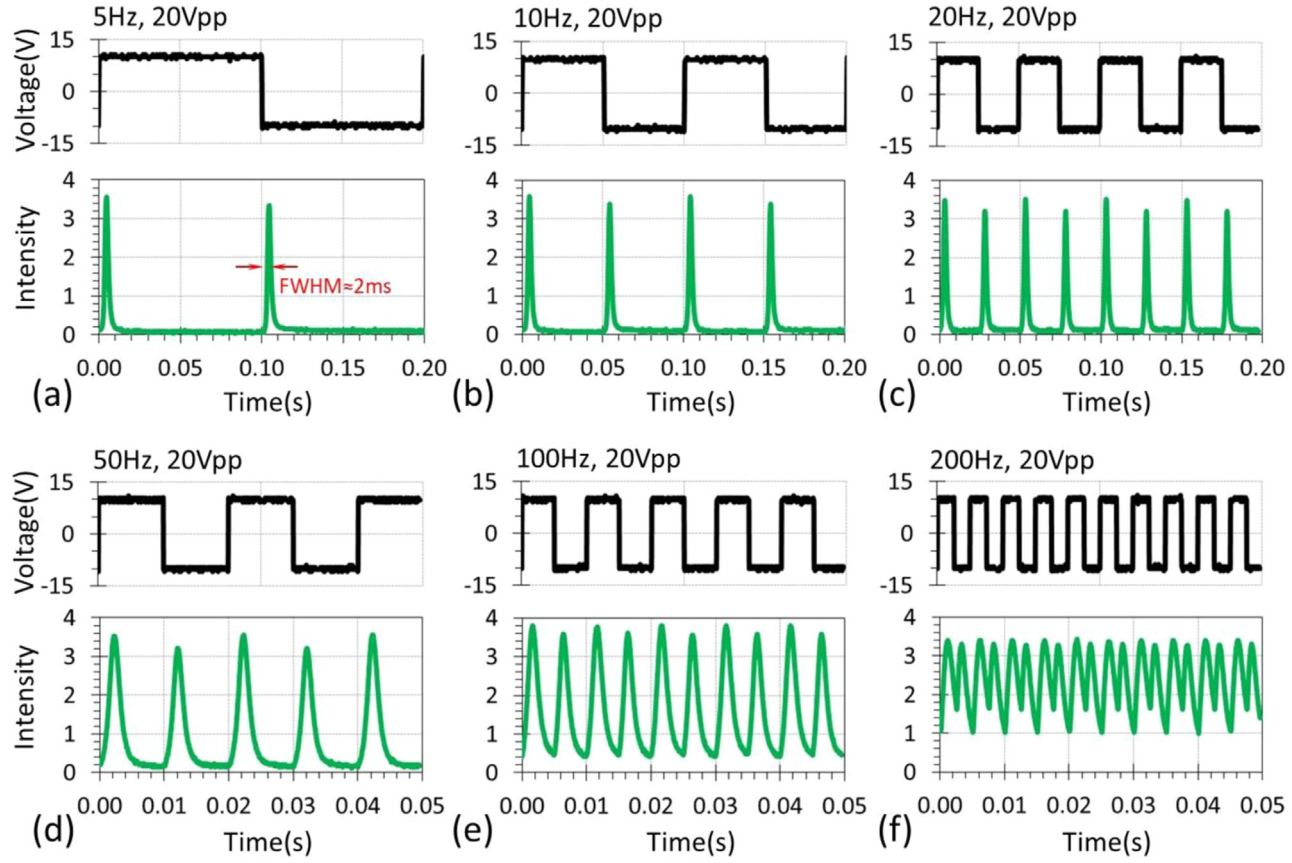

Fig. 9. Measured optical intensity signal (in green) at varying frequencies of the 20 Vpp voltage signal (in black) addressed to the FLC modulator in between crossed polarizers, with the input polarizer parallel to the first stable LC orientation.

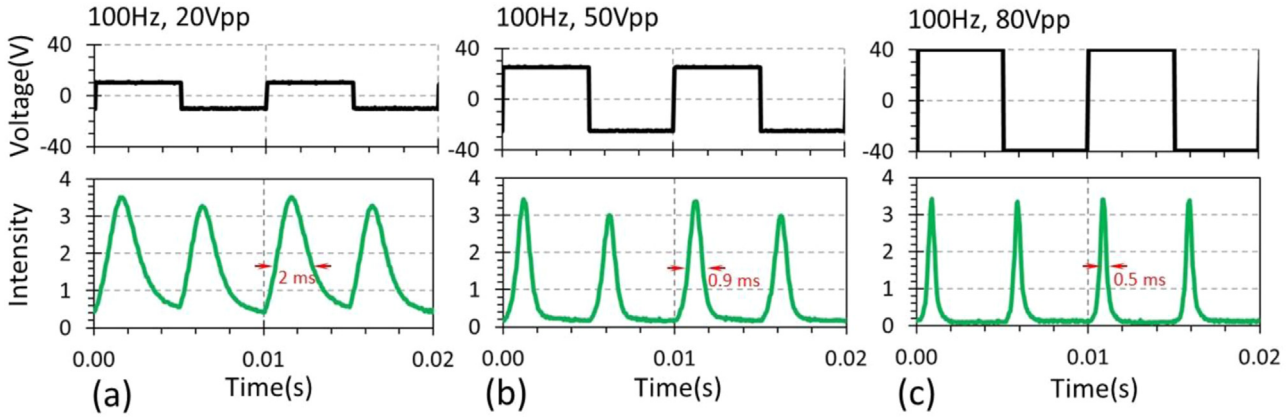

Fig. 10. Comparison of the optical intensity for addressed voltage signals of 100 Hz with (a) 20 Vpp, (b) 50 Vpp and (c) 80 Vpp.

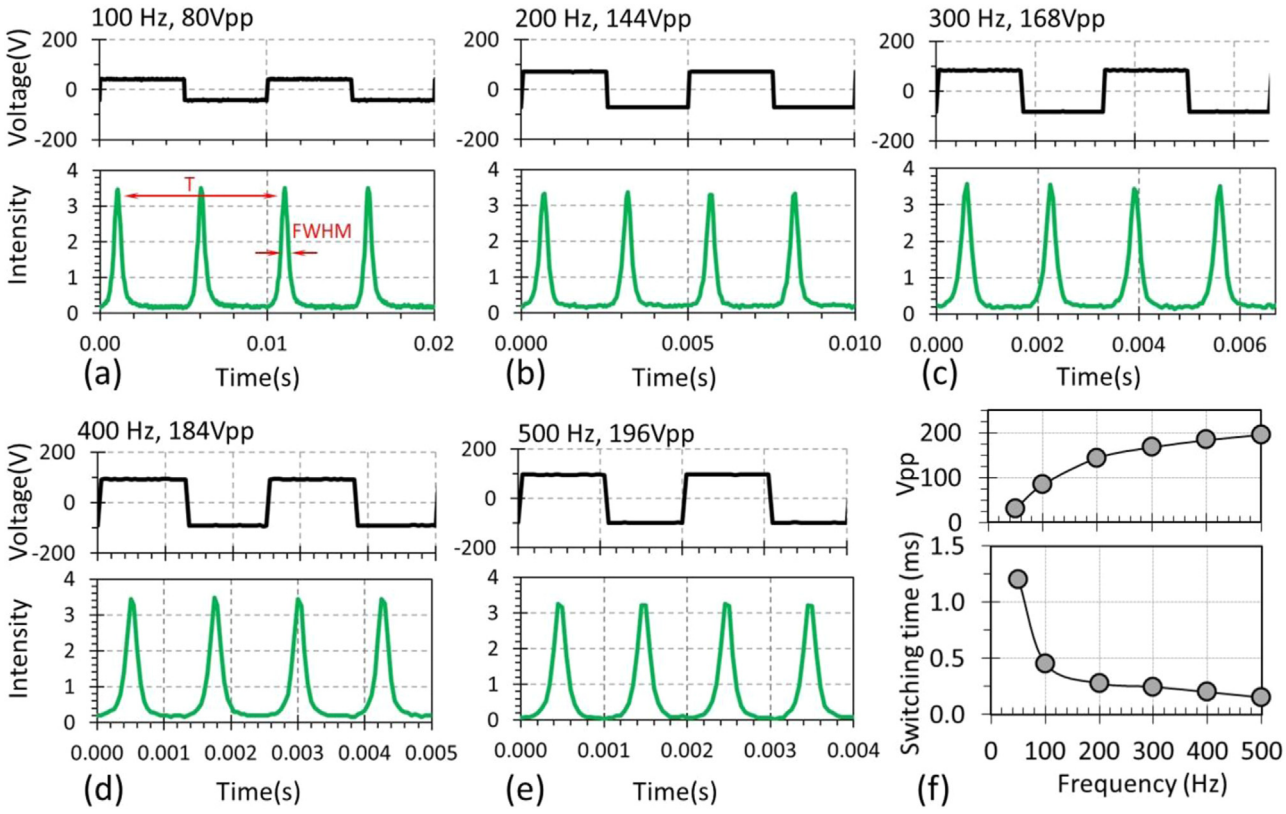

Fig. 11. (a)-(e) Measured optical intensity signal (in green) at varying frequencies. The Vpp value of the voltage signal (in black) is adjusted in each case to provide a ratio $FWHM/T < 1/10$. (e) Required Vpp versus frequency. (f) Measured switching time versus frequency.

on the output optical signal. In these experiments the FLC modulator was placed between crossed polarizers, with the first polarizer parallel to the first stable orientation of the LC director. In this situation the intensity for the two stable states is very low, since the SOP that exits the FLC cell is perpendicular to the analyzer. The change in the LC orientation is visible in the form of transition peaks that approach the maximum 100% normalized transmission. These peaks occur when, on its transition from stable position A to B, the LC director becomes horizontally aligned.

Fig. 9 shows the captured optical intensity signal for frequencies of 5, 10, 20, 50, 100 and 200 Hz. Here the intensity captures are not normalized to better see the effect when increasing the frequency, and the figures show the voltage signal directly measured in the photodetector (green curves). Below 50 Hz the difference between the two stable states is minimal and the transmission at the stable states remains very low. The transition peaks reach the maximum value, with full width at half maximum ($FWHM$) slightly less than 2 ms in all cases. For 100 Hz the optical signal does not reach the lowest value. The optical signal shows a significant degradation for 200 Hz, thus implying that the FLC director does not fully switch through the expected angle of $\phi = 90^{\circ}$ between the two stable states. This simple procedure therefore reveals that we must consider 50 Hz as the proper frequency limit for the effective operation of the FLC cell when addressing a 20 Vpp signal.

However, we can overcome this degradation by increasing the amplitude of the applied voltage signal. The response time or switching time of the FLC cell is expected to lower as the amplitude increases. This is illustrated in Fig. 10 for the frequency of 100 Hz. We show here the data already shown in Fig. 9 (with 20 Vpp) with new captures obtained with 50 Vpp and 80 Vpp. The switching time, measured as the $FWHM$ of the transient peaks, is reduced below the millisecond.

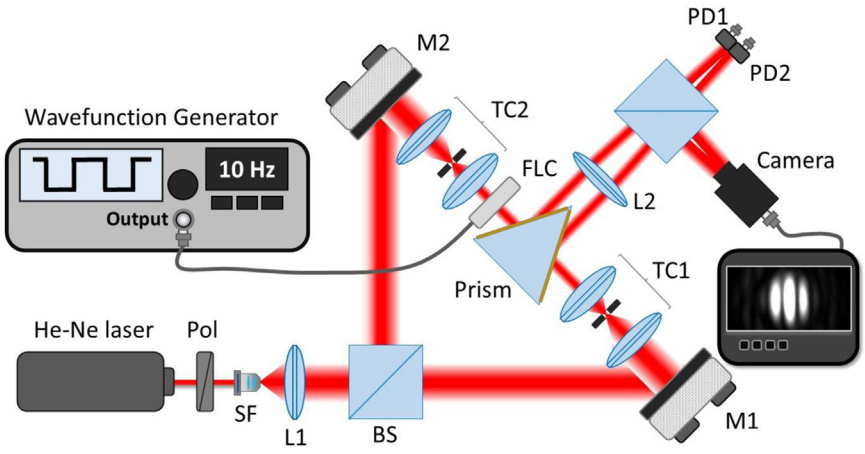

Fig. 12. Scheme of the interferometer setup for measuring the phase modulation. SF: spatial filter; L1: collimating lens; L2 Fourier transform lens; BS: beam-splitter; TC: telescope system; M: mirror; PD: photodetector.

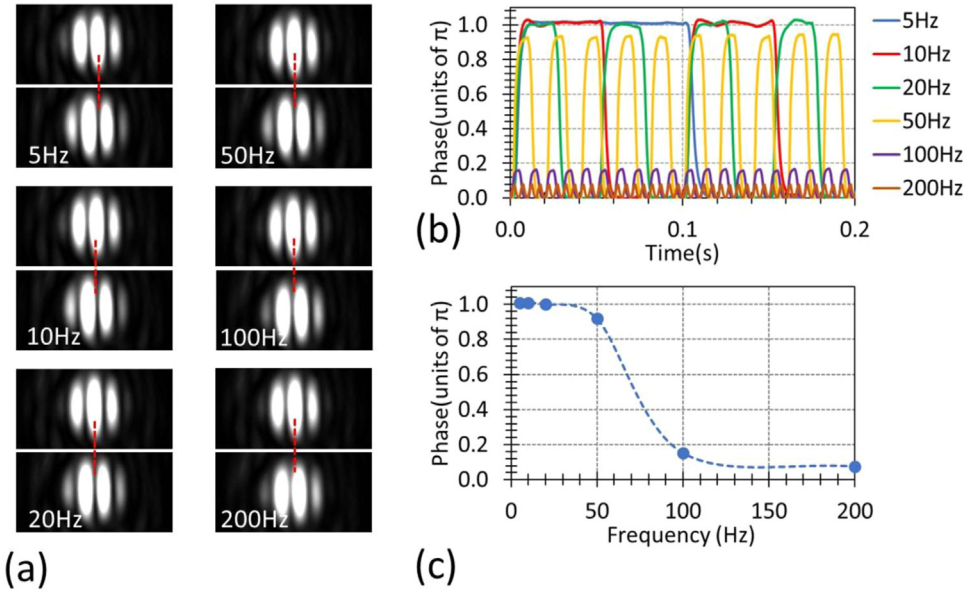

Fig. 13. (a) Interference patterns for the FLC modulator illuminated with horizontal linear polarization for different frequencies of the addressed voltage signal of 20 Vpp and for the two stable states of the FLC. (b) Measured phase modulation at varying frequencies. (c) Maximum phase shift versus frequency.

Therefore, operation at higher frequencies is possible by applying larger voltages. This is demonstrated in Fig. 11, where we present results up to 500 Hz. For each frequency, the voltage amplitude is increased to reach approximately a ratio $FWHM/T < 0.1$ between the switching time and the period (T) of the addressed signal. Figs. 11(a) to 11(e) show transmission peaks with similar relative width with respect to their time interval. Note that the time scale is different in every figure to display only four peaks of each signal. Fig. 11(f) shows the Vpp value that must be applied for each frequency to achieve this situation, and how the switching time progressively diminishes. The result in Fig. 11(e) shows a good optical signal with a switching time close to FWHM=0.2 ms for an addressed voltage of 500 Hz and 196 Vpp. Although these are too high voltage values for practical devices, which require the minimum switching time and must use low voltage FLC mixtures [41], these results illustrate how the device can be operated at different frequencies.

6. Characterization of the phase modulation

The characterization of the FLC modulator optical properties is completed in this section by verifying the expected binary π phase modulation for all polarization states. Despite the fabricated FLC modulator does not fulfill exactly the ideal parameters ($\phi = 180^\circ$ and $\theta = 90^\circ$), we show next that this phase modulation regime is reproduced quite well.

The phase shift between the two stable states of the FLC modulator was experimentally retrieved with a very versatile specially-adapted Young's interferometer which detects the optical interference pattern by a bicell photo-detector in a back Fourier focal plane [28]. Fig. 12 shows a scheme of this interferometer setup intended to provide time-resolved measurements of the phase modulation. In addition to the ordinary camera-based interferometry, which has limited capturing rate and long processing time for fringe pattern, the bicell detector-based interferometry technique provides enough sampling rate along the time axis. The experimental setup uses a beam-splitter to divide the linearly polarized and spatially filtered beam of a He-Ne laser in a reference and a probe beam. The beam reflected in mirror M1 is the reference beam and that reflected in mirror M2 is the probe beam. The FLC cell was placed in the arm of the probe beam and is reflected on one side of a gold coated right angle prism alongside the reference beam on the opposite side of the prism. The reflected rays from both sides of the prism propagate parallel to each other separated by a distance dependent on the dimensions of the prism. The beams are then combined by a converging lens (L2) to provide the Fourier transform where the interference pattern is observed at the back focal plane, where two photo-detectors are placed. The photodetectors are separated from each other by a distance gap equivalent to that of the two beams being reflected from the prism. For purposes of simultaneously visualizing the interference pattern on a camera we place a beam splitter right after the prism and lens L2.

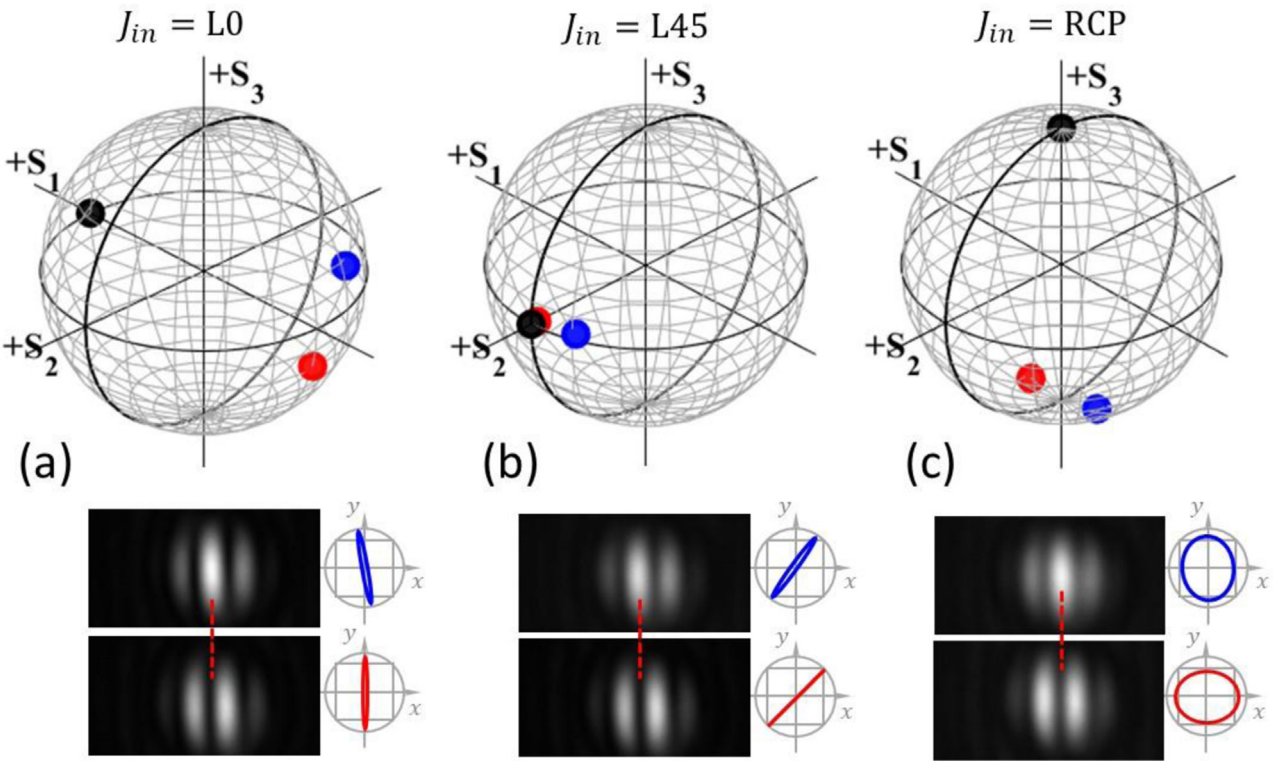

Fig. 14. Transformations of SOP in the PS for the FLC with real parameters $\phi = 164^{\circ}$ and $\theta = 85^{\circ}$ for input SOPs (a) L0, (b) L45 and (c) RCP. Below each case the experimental interference patterns are shown for the two SOP emerging from the FLC modulator.

Table 1
Stokes parameters and ellipticity and azimuth angles expected for the two emerging states of the FLC modulator for three different input SOP.

Input SOP	Output Stokes parameters State A			Output Stokes parameters State B			Ellipticity angle (degrees)		Azimuth Angle (degrees)	
	S_1	S_2	S_3	S_1	S_2	S_3	A	B	A	B
L0	−0.96	0.00	−0.28	−0.90	−0.34	0.28	−8.0	7.9	90.0	−79.8
L45	0.00	1.00	0.00	−0.33	0.94	0.05	0.0	1.4	45.0	54.8
RCP	0.28	0.00	−0.96	−0.27	−0.05	−0.96	−37.0	−37.0	0.0	−85.0

Fig. 13 shows a set of experiments where the FLC cell was illuminated with horizontal linearly polarized light. Again, the modulator was addressed with a bipolar square voltage signal of 20 Vpp and varying frequency (5, 10, 20, 50, 100 and 200 Hz). Fig. 13(a) presents the interference patterns captured on the camera for every frequency of the applied voltage. For each case, two interferograms are presented, corresponding to the two stable states of the FLC modulator. For low frequencies, up to 50 Hz, the interference contrast clearly reverses from each interference pattern (a red discontinuous line was drawn to clearly visualize this effect), thus indicating a π-phase difference between the two FLC states. At higher frequencies, as expected from the previous results in Section 5, the interference pattern does not show contrast inversion.

This is further demonstrated in Fig. 13(b) through quantitative, and time resolved measurements of the phase modulation. For frequencies of 5, 10 and 20 Hz the phase modulation perfectly reproduces a binary function with a π phase shift. At 50 Hz the maximum phase shift does not recover the maximum value, reaching slightly 0.9π As the frequency increases, the binary phase modulation regime is lost and there is a progressive reduction of the maximum phase difference, with values below 0.2π for 100 Hz and below 0.1π for 200 Hz. Fig. 13(c) shows the evolution of the maximum phase shift versus frequency.

Finally, Fig. 14 presents another set of equivalent interferograms for three different input states of polarization: a linear horizontal state, a linear state oriented at 45°, and the RCP state. Here we apply a square voltage signal of 20 Vpp and 5 Hz, so the frequency limit is very far. Fig. 14 shows first the representation on the PS of the input SOP and the two expected emerging SOPs, where the measured FLC physical parameters $\phi = 164$ and $\theta = 85^{\circ}$ were considered in the simulations. The two emerging states have similar SOP and give two very close but different points on the PS. For each input SOP, Table 1 gives the expected SOP in terms of their Stokes parameters as well as their ellipticity and azimuth angles. The polarization ellipses of these states are drawn next to the interferogram patterns.

Since the SOP difference is very small, the interferograms are expected with very good visibility. The second row of Fig. 14 shows, for each input SOP, the two interference patterns captured for each stable position (A and B) of the FLC modulator. The three cases verify the good visibility and the contrast inversion of the interference, thus demonstrating a π phase-shift that is obtained independently of the input state.

7. Conclusions

In summary, we have fabricated a FLC modulator with a large switching rotation angle close to 90° and retardance around 180° (HWP regime) for a wide visible spectral range. Physico-chemical properties of the specific LC mixture used to fabricate the FLC modulator with such large tilt angle were provided. In addition, a reverse engineering procedure was performed for the precise and unambiguous verification of its physical parameters (location of the liquid-crystal director, its sense of rotation upon applying a square voltage signal, and spectral retar-

dance function). An experimental analysis of the frequency limits of the fabricated device has been also included. Finally, the phase modulation properties of the modulator were experimentally probed, and the expected binary π phase-shift was verified for various input polarization states.

Although this principle of operation was proposed years ago [22–25], it has barely been implemented, probably due to the difficult realization of FLC modulators with such large switching rotation angles. The application of this scheme to FLC spatial light modulators could be very interesting, since they would be binary phase modulators with the highest diffraction efficiency and useful for all states of polarization, therefore including unpolarized light, a situation that is not possible with the common nematic LC -SLMs or with standard FLC-SLMs of smaller rotation angles.

Declaration of Competing Interest

The authors declare that they have no known competing financial interests or personal relationships that could have appeared to influence the work reported in this paper.

CRediT authorship contribution statement

Esther Nabadda: Investigation, Visualization, Writing – original draft. **Noureddine Bennis:** Conceptualization, Methodology, Validation, Writing – review & editing. **Michał Czerwinski:** Methodology, Validation. **Aleksandra Walewska:** Investigation, Visualization. **Leszek R. Jaroszewicz:** Supervision. **María del Mar Sánchez-López:** Methodology, Validation, Writing – review & editing. **Ignacio Moreno:** Conceptualization, Validation, Supervision.

Acknowledgements

This work received financial support from Ministerio de Ciencia, Innovación y Universidades, Spain (grant project RTI2018–097107-B-C33), from Wojskowa Akademia Techniczna, Poland (UGB 22–791) and from European Social Fund (NAWA PROM project POWR.03.03.00–00-PN13/18). E.N. acknowledges a grant from Generalitat Valenciana, Santiago Grisolia Program (ref. GRISOLIAP/2020/004).

References

[1] Moddel G. Ferroelectric liquid crystal spatial light modulators. Spatial Light Modulator Technology: Materials, Devices and Applications Chap 6. New York: U Efron Edt Marcel Dekker Inc; 1994.
[2] Gros E, Dupont L. Ferroelectric liquid crystal optical waveguide switches using the double-refraction effect. IEEE Photon. Technol. Lett. 2001;13(2):115–17.
[3] Manolis IG, Wilkinson TD, Redmond MM, Crossland WA. Reconfigurable multilevel phase holograms for optical switches. IEEE Photon. Technol. Lett. 2002;14(15):801–3.
[4] Sirleto L, Coppola G, Breglio G, Abbate G, Righini GC, Otón JM. Electro-optical switch and continuously tunable filter based on a Bragg grating in a planar waveguide with a liquid crystal overlayer. Opt. Eng. 2002;41(47):2890–8.
[5] Hariharan P, Ciddor PE. Improved switchable achromatic phase shifters. Opt. Eng. 1999;38(6):1078–80.
[6] Peinado A, Lizana A, Campos J. Use of ferroelectric liquid crystal panels to control state and degree of polarization in light beams. Opt. Lett. 2014;39(3):659–62.
[7] Jaulin A, Bigué L, Ambs P. High-speed degree-of-polarization imaging with a ferroelectric liquid-crystal modulator. Opt. Eng. 2008;47(3):033201.
[8] Peinado A, Lizana A, Iemmi C, Campos J. Polarization imaging with enhanced spatial resolution. Opt. Commun. 2015;338:95–100.
[9] Mukherjee S, Yuan Z, Sun Z, Li A, Kang C, Kwok H, Srivastava AK. Fast refocusing lens based on ferroelectric liquid crystals. Opt. Express 2021;29(6):8258–67.
[10] Yuan Z, Sun Z, Kwok H, Srivastava AK. Fast LiDAR systems based on ferroelectric liquid crystal dammann grating. Liq. Cryst. 2021;48(10):1402–16.
[11] Guo Q, Yan K, Chigrinov V, Zhao H, Tribelsky M. Ferroelectric liquid crystals: physics and applications. Crystals 2019;9(9):470–90.
[12] Bougrenet de la Tocnaye JL, Dupont L. Complex amplitude modulation by use of a liquid crystal spatial light modulators. Appl. Opt. 1997;36:1730–41.
[13] Martínez A, Beaudoin N, Moreno I, Sanchez-López MM, Velasquez P. Optimization of the contrast ratio of a ferroelectric liquid crystal optical modulator. J. Opt. A: Pure Appl. Opt. 2006;8(1):1013–18.
[14] Gourlay J, Samus S, McOwan P, Vass DG, Underwood I, Worboys M. Real-time binary phase holograms on a reflective ferroelectric liquid-crystal spatial light modulator. Appl. Opt. 1994;33:8251–4.
[15] Le Doucen M, Pellat-Finet P. Polarization properties and diffraction efficiencies of binary anisotropic gratings: general study and experiments on ferroelectric liquid crystals. Opt. Commun. 1998;151:321–30.
[16] Forth Dimension Displays, 2022 https://www.forthdd.com/.
[17] Tong Z, Chen X. A ferroelectric liquid crystal spatial light modulator encoded with orthogonal arrays and its optimized design for laser speckle reduction. Opt. Laser Eng. 2017;90:173–8.
[18] Förster R, Lu-Walther HW, Jost A, Kielhorn M, Wicker K, Heintzmann R. Simple structured illumination microscope setup with high acquisition speed by using a spatial light modulator. Opt. Express 2014;22(17):20663–77.
[19] Schlichenmeyer TC, Wang M, Elfer KN, Brown JQ. Video-rate structured illumination microscopy for high-throughput imaging of large tissue areas. *Biomed. Opt. Express* 2014;5(2):366–77.
[20] Schmieder F, Klapper SD, Koukourakis N, Busskamp V, Czarske J. Optogenetic stimulation of human neural networks using fast ferroelectric spatial light modulator-based holographic illumination. Appl. Sci. 2018;8:1180.
[21] Martínez-García A, Moreno I, Sánchez-López MM, García-Martínez P. Operational modes of a ferroelectric LCoS modulator for displaying binary polarization, amplitude, and phase diffraction gratings. Appl. Opt. 2009;48(15):2903–14.
[22] O'Callaghan MJ, Handschy MA. Diffractive ferroelectric liquid-crystal shutters for unpolarized light. Opt. Lett. 1991;16(10):770–2.
[23] TWarr S, Mears RJ. Polarisation insensitive operation of ferroelectric liquid crystal devices. Electron. Lett. 1995;31:714–16.
[24] Warr ST, Mears RJ. Polarisation insensitive diffractive FLC systems. Ferroelectrics 1996;181(1):53–9.
[25] Brown CV, Kriezis EE. Calculation of the efficiency of polarization-insensitive surface-stabilized ferroelectric liquid-crystal diffraction gratings. Appl. Opt. 2003;42(13):2257–63.
[26] Manolis IG, Redmond MM, Crossland WA, Davey AB, Wilkinson TD. Control of the electro-optic bistability of some ferroelectric liquid crystals useful for binary phase optical modulators. Mol. Cryst. Liq. Cryst. 2000;351:305–14.
[27] Ma Y, Tam AMW, Gan XT, Shi LY, Srivastava AK, Chigrinov V, Kwok HS, Zhao JL. Fast switching ferroelectric liquid crystal Pancharatnam-Berry lens. Opt. Express 2019;27(7):10079–86.
[28] Bennis N, Merta I, Kalbarczyk A, Maciejewski M, Marc P, Spadlo A, Jaroszewicz LR. Real time phase modulation measurements in liquid crystals. Opto Elect. Rev. 2017;25(2):69–73.
[29] Sánchez-López MM, García-Martínez P, Martínez-García A, Moreno I. Poincaré sphere analysis of a ferroelectric liquid crystal optical modulator: application to optimize the contrast ratio. J. Opt. A Pure Appl. Opt. 2009;11:015507.
[30] Matsumoto T, Fukuda A, Johno M, Motoyama Y, Yui T, Seomunc S, Yamashita M. A novel property caused by frustration between ferroelectricity and antiferroelectricity and its application to liquid crystal displays - Frustoelectricity and V-shaped switching. J. Mater. Chem. 1999;9(9):2051–80.
[31] Kurp K, Czerwiński M, Salamon P, Bubnov A, Tykarska M. Design of functional multicomponent liquid crystalline mixtures with nano-scale pitch fulfilling deformed helix ferroelectric mode demands. J. Mole. Liq. 2019;290:111329 1-10.
[32] Drzewiński W, Czupryński K, Dąbrowski R, Neubert M. New antiferroelectric compounds containing partially fluorinated terminal chains. Synthesis and mesomorphic properties. Mol. Cryst. Liq. Cryst. 1999;328:401–10.
[33] Chandrasekhar S. Liquid Crystals. Cambridge University Press; 1977. p. 10. P.
[34] Tykarska M, Czerwiński M, Miszkurka J. Influence of temperature and terminal chain length on helical pitch in homologue series nH6Bi. Liq. Cryst. 2010;37(4):487 49.
[35] Czerwiński M, Tykarska M. Helix parameters in bi- and multicomponent mixtures composed of orthoconic antiferroelectric liquid crystals with three ring molecular core. Liq Cryst 2014;41(6):850–8.
[36] Kuczynski W, Lagerwall T, Matuszczyk M, Skarp K, Stebler B, Wahl J. Fast-switching low-temperature liquid crystal mixtures. Mol. Cryst. Liq. Cryst. 1987;146:173–87.
[37] Abdulhalim I, Moddel G, Clark NA. Director-polarization reorientation via solitary waves in ferroelectric liquid crystals. Appl. Phys. Lett. 1992;60(5):551–3.
[38] Abdulhalim I, Moddel G, Clark NA. Soliton switching in ferroelectric liquid crystals and their transient electro-optic response. J. Appl. Phys. 1994;76(2):820–31.
[39] Abdulhalim I. Continuous phase-only or amplitude light modulation using ferroelectric liquid crystals with fixed boundary orientations. Opt. Commun. 1994;108:219–24.
[40] Messaadi A, Sánchez-López MM, García-Martínez P, Vargas A, Moreno I. Optical system for measuring the spectral retardance function in an extended range. J. Eur. Opt. Soc. Rapid Pub. 2016;12(21):1–9.
[41] Hughes JR, Bannister RW, Graham A, McDonnell DG, Pedlingham HA, Scattergood DC, Smith CJT. A high resolution ferroelectric liquid crystal display. Displays 1994;15(2):117.